

Dynamic Compression of Earth Materials

Thomas J. Ahrens

The first measurements of the dynamic compression of earth materials, carried out for two different gabbros and a dunite, were reported to pressures of 75 gigapascals (0.75 megabar) (1) by Hughes and McQueen of Los Alamos Scientific Laboratory in 1958 (2). This pioneering study, which demonstrated that the pressure-density characteristics of the upper mantle could be closely ap-

proximated by a dunite of composition $(\text{Mg}_{0.9}\text{Fe}_{0.1})_2\text{SiO}_4$, also showed that shock-induced polymorphism of silicate minerals could take place on the sub-microsecond time scale of shock wave experiments. Hughes and McQueen's paper presented the first pressure-density data for earth materials in a pressure regime significantly above the level of ~ 10 GPa explored by Bridgman (3) almost a decade earlier. The techniques

Summary. Shock wave techniques have been used to investigate the pressure-density relations of metals, silicates, and oxides over the entire range of pressures present in the earth (3.7×10^6 bars at the center). In many materials of geophysical interest, such as iron, wüstite, calcium oxide, and forsterite, major shock-induced phase changes dominate the compression behavior below pressures of 10^6 bars. The shock wave data for the high-pressure phases of these minerals lead to important inferences about the composition of the lower mantle and outer, liquid core of the earth. The lower mantle of the earth appears to have a slightly higher density than is inferred to correspond to the behavior of an olivine-rich assemblage of the same composition as the upper mantle. The core has a density some 10 percent less than that of pure iron and may have 9 to 12 percent sulfur or about 8 percent oxygen by weight.

ported shock wave data for iron and several other metals to pressures of 400 GPa. Since the center of the earth is at a pressure of 370 GPa, the ability to study the behavior of materials throughout the entire pressure range present in the earth by dynamic compression techniques was thus firmly demonstrated.

they used, involving explosively driven shock waves, were first described in connection with studies of the shock compression of five metals in 1955 (4) and were an outgrowth of engineering research on the atomic bomb at Los Alamos.

As early as 1954, an unusually significant result of the Los Alamos group's effort was reported by Minshall (5), who

described a shock-induced phase change in pure iron occurring at 13 GPa. The crystallographic nature of the high-pressure (ϵ) phase is the hexagonal close-packed structure with a (zero pressure) density of 8.32 grams per cubic centimeter, compared to the value of 7.875 g/cm³ for the normal body-centered cubic phase. However, this structure was not suggested until 1962, when Jamieson and Lawson (6) proposed it on the basis of one x-ray diffraction line obtained in an early version of a static high-pressure, x-ray apparatus (7). In 1958, Al'tshuler and co-workers (8) in the Soviet Union re-

ported shock wave data for iron and several other metals to pressures of 400 GPa. Since the center of the earth is at a pressure of 370 GPa, the ability to study the behavior of materials throughout the entire pressure range present in the earth by dynamic compression techniques was thus firmly demonstrated.

Although the study of shock or dynamic compression of rocks and minerals has largely been motivated by a need to compare the pressure-density and pressure-sound speed relations of mantle and core minerals with seismic data for the earth, as emphasized in the present article, other technical applications of this area of research exist. Since the discovery that polycrystalline graphite, on being subjected to shock compression, will in some cases produce more than 50 percent polycrystalline diamond which is recoverable (9), considerable research has centered on the shock-induced phase changes in such minerals as graphite (10), fluorite (11), cassiterite (12), rutile (11, 13), and quartz (14). Pressure-density data from shock wave experiments have demonstrated that transformation under dynamic compression can occur on a time scale of microseconds. These phases have also been recovered from high-pressure diamond anvil-laser heating experiments (15). Other technical and military applications of shock wave research on rocks are related to their dynamic yielding properties, which are important in the physics of large-scale excavation by nuclear explosives (16), detection and teleseismic monitoring of underground nuclear explosions (17), and prediction of the response of buried strategic structures to explosively induced ground shock (18).

Experimental Methods

In most shock wave experiments designed to measure properties of materials under dynamic compression, a planar shock is propagated into a sample through what is often referred to as a base plate (Fig. 1). This, in turn, is in contact with a detonating chemical or a nuclear explosive assembly (Fig. 1, a and

The author is a professor of geophysics at the Seismological Laboratory, Division of Geological and Planetary Sciences, California Institute of Technology, Pasadena 91125.

Table 1. Shock-induced phase changes of geophysical importance.

Low-pressure phase		High-pressure phase		
Material	Density* (g/cm ³)	Structure	Density* (g/cm ³)	Reference
<i>Core materials</i>				
Iron, body-centered cubic, Fe	7.875	Hexagonal close-packed	8.32	(53)
Iron-nickel (10%), body-centered cubic, Fe _{0.9} Ni _{0.1}	7.884, 7.86	Hexagonal close-packed	8.33	(54)
Pyrrhotite, Fe _{0.94} S	4.603	?	5.3-5.5	(52)
Pyrite, FeS ₂	4.61	?	5.3	(52, 55)
Wüstite, Fe _{0.94} O	5.50	?	5.84	(51)
3Fe ₃ Si + FeSi	7.016	Hexagonal close-packed	7.46	(48)
Fe ₃ Si + FeSi	7.646	Hexagonal close-packed	8.51	(48)
Magnetite, Fe ₃ O ₄	5.12	FeO (LS) + Fe ₂ O ₃ (LS) [†]	6.4	(12, 56)
Hematite, Fe ₂ O ₃	5.00	Corundum (LS)	6.05	(12, 56)
<i>Mantle materials</i>				
Periclase, MgO	3.58	None		(12)
Corundum, Al ₂ O ₃	3.98	None		(12)
Quartz, SiO ₂	2.65	Rutile	3.248	(12, 57)
Bronzite, (Mg _{0.92} , Fe _{0.08})SiO ₃	3.34	Hypothetical perovskite	4.20	(45, 56)
Forsterite, Mg ₂ SiO ₄	3.32	Hypothetical perovskite + rock salt	3.93	(38)
Dunite, (Mg _{0.88} , Fe _{0.12}) ₂ SiO ₄	3.55	Hypothetical perovskite + rock salt	4.04	(45)
Garnet, (Fe _{0.79} , Mg _{0.14} , Ca _{0.04} , Mn _{0.03})Al ₂ Si ₃ O ₁₂	4.18	?	~ 4.4	(30)
Spinel, MgAl ₂ O ₄	3.582	Orthorhombic	4.31	(43, 56)
Dunite, (Mg _{0.45} , Fe _{0.55}) ₂ SiO ₄	3.85	Hypothetical perovskite + rock salt	4.62	(12, 45)
Calcite, CaO	3.35	CsCl	3.71	(44)

*Values are for 1 bar and 25°C. †LS, Fe²⁺ assumed to be in a low-spin orbital configuration.

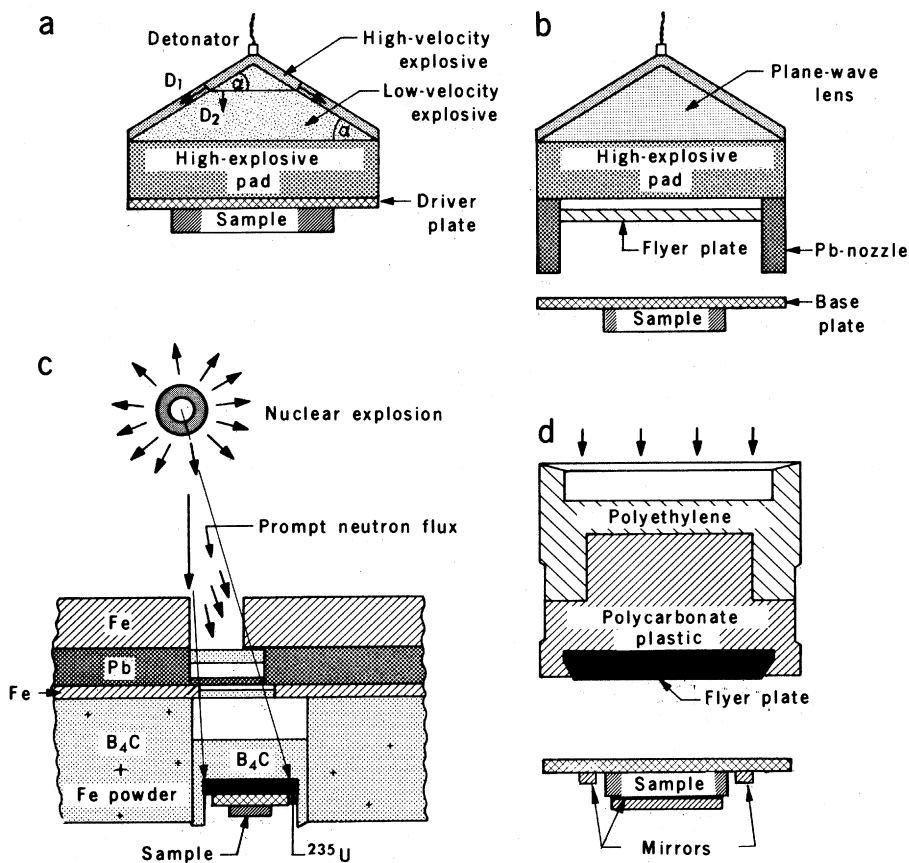


Fig. 1. Shock generating methods. (a) Point detonation of an explosive (lens) configuration (10 to 30 cm in diameter) constructed of explosives with fast (D_1) and slow (D_2) detonation velocities produces a planar detonation in an underlying explosive pad (for example, TNT) if $D_2 = D_1 \sin \alpha$. The resulting shock wave propagates through the base plate into the sample (19). In aluminum, shock pressures of ~25 GPa (0.25 Mbar) result if TNT is used. (b) A plane-wave detonated explosive pad accelerates the metal flyer plate to ~4.5 km/sec to impact the sample assemblies (19). With an iron flyer plate, pressures up to 140 GPa (1.4 Mbar) are achieved in copper base plates. (c) Prompt neutrons from a nuclear explosion nearly uniformly irradiate a ²³⁵U plate, causing internal fission-induced heating. The resulting rapid expansion (explosion) of the ²³⁵U plate drives an intense shock into the base plate and sample. Pressures of 2 TPa (20 Mbar) have been induced in molybdenum by this method (58). (d) By using a light-gas (H₂) gun (Fig. 3), 20-gram projectiles are launched at 7 km/sec and impact samples 1 cm in diameter and 3 mm thick, inducing shock pressures up to ~ 5 GPa (5 Mbar) (21).

c) or is impacted by a flyer plate which is launched explosively or with a gun (Fig. 1, b and d). In these experiments the two kinematic parameters of the one-dimensional flow (Fig. 2) usually measured are the shock velocity, U , and particle velocity, u ; these, when taken with the initial density, ρ_0 , and the Rankine-Hugoniot relations for the conservation of mass, momentum, and internal energy across the shock front (19)

$$\rho = \rho_0 U / (U - u)$$

$$P = \rho_0 u U$$

$$\Delta E = E_1 - E_0 = P (1/\rho_0 - 1/\rho)/2$$

permit solution for the thermodynamic properties P , ρ , and ΔE of the shock state. Here P is the shock pressure and ΔE is the change in internal energy density.

In most experiments the shock velocity is obtained by measuring the time difference between the entrance and exit of the shock front through a sample. In the light-gas gun of Figs. 1 and 3, the shock transit time through a sample 3 millimeters thick may be as short as 200 nanoseconds (2×10^{-7} second), whereas for nuclear explosive sources, samples 60 to 120 millimeters thick provide travel times of ~ 3 to 5 microseconds (20). In general, for useful results shock velocity (time interval) measurements must be made with precisions better than 1 percent. These can be achieved by using the streak camera methods demonstrated in Figs. 3 and 4, or by electrical pin contactor techniques (21). In the simple case where the flyer plate, driver plate, and sample are all made of the same material, the particle or mass velocity u , relative to the usual laboratory frame of reference, is equal to one-half of the projectile velocity. When the flyer plate and sample are of different materials, the particle velocity is determined by what is termed the impedance match method (19), which relies on continuity of stress and particle velocity at the flyer-sample interface.

The parameters P , ρ , and u which describe the high-pressure shock state can,

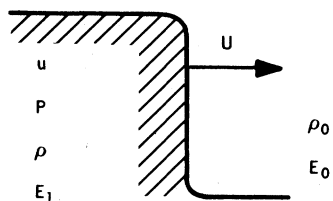


Fig. 2. Profile of a steady shock wave imparting a particle velocity u , pressure P , density ρ , and internal energy density E_1 , propagating with velocity U into material that is at rest at density ρ_0 and internal energy density E_0 .

and have, been directly measured as well (19, 22). In nonmetallic samples below shock stresses of ~ 40 GPa, both the shock pressure and the particle velocity are determined (as functions of time) by constructing the target assembly so that it includes a typical (0.1 mm) thick wire or foil made of manganin alloy, which is placed in the plane of the shock. The increased resistance of manganin when subjected to shock or hydrostatic pressures provides a direct measurement of dynamic pressure (19). Also, by placing a wire within the plane of the shock perpendicular to an impressed magnetic field, a voltage is generated which is proportional to the shock-induced particle velocity. Particle velocities of nearly 3 kilometers per second have been measured with such a configuration. It is important to point out that regardless of whether shock velocity, particle velocity,

or pressure is measured to determine the peak shock state, generally only one such state, termed the Hugoniot state, is measured in a single (expendable) sample during an experiment, although several samples are often mounted on a single base plate.

Shock temperatures are also currently being determined for an increasing number of transparent substances by measuring the radiation spectrum (nearly a blackbody spectrum) of the hot material behind the shock front in the interval of 0.2 to 0.5 μsec when strong shock waves propagate through samples (23).

Relation of Shock Wave Data to

Other Data

The locus of peak shock states that are achieved from some initial state is defined as the Hugoniot curve. The relation of the Hugoniot curve to other thermodynamically defined pressure-density curves is shown in Fig. 5. With the notable exception of Al_2O_3 (corundum), MgO (periclase), and MnO_2 (pyrolusite) (12), most of the elements, oxides, and silicates and many of the compounds and alloys of geophysical interest that have been tested to date show dramatic evidence of shock-induced transitions or phase changes in the currently accessible pressure regime. In addition to the materials listed in Table 1, major shock-in-

duced phase changes are observed in all alkali halides initially in the NaCl structure (including halite), the carbonate minerals, graphite, fluorite, rutile, cassiterite, plagioclases, topaz, ilmenite, sulfate minerals, barite, sphalerite, andalusite, sillimanite, serpentine, and jadeite.

Before I discuss the relation of the thermodynamic state produced in shock compression experiments to other data, two not unrelated problems need to be addressed: (i) the rheological properties of shock-compressed minerals and (ii) the degree to which shock states can be assumed to be in thermodynamic equilibrium. The shock stress level at which dynamic yielding occurs under the conditions of one-dimensional strain is termed the Hugoniot elastic limit (HEL) (Fig. 5). At stresses below this level, which may be as high as 20 GPa for shock propagation along the [001] direction in corundum or as low as 0.03 GPa for propagation along the [100] direction in halite (24), the deformation induced by shock waves can be considered equivalent to that achieved by finite-strain longitudinal elastic waves. Above the HEL, deformation takes place on a microscopic level as the result of dynamic yielding in the shock front. As indicated in Fig. 5, neglecting thermal effects, the degree to which the shock states differ from the pressure-density "hydrostat" (a theoretical Hugoniot curve, constructed from

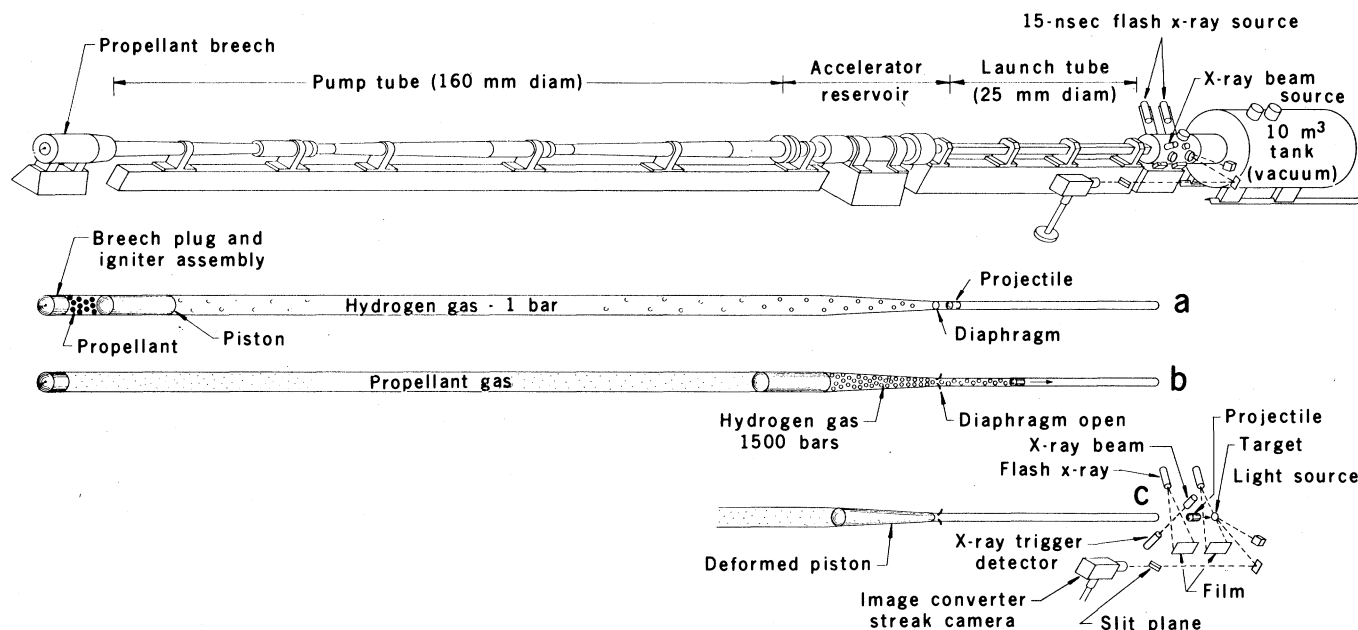


Fig. 3. Diagrammatic view of the Caltech two-stage light-gas gun used for shock wave research on earth materials. The total length of the apparatus is 33 m, total mass approximately 35 tons. (a) When the chemical propellant ignites, a 20-kg plastic piston compresses hydrogen in the pump tube. (b) As the projectile enters the high-pressure reservoir section, the diaphragm ruptures and the projectile begins to accelerate down the launch tube. (c) As a result of the deformation of the plastic piston in the high-pressure reservoir, gas pressure is maintained on the base of the projectile as it is accelerated, until it clears the launch tube. After leaving the launch tube, the projectile, which usually has a tantalum plate in its nose, intersects a continuous x-ray beam and triggers two 15-nanosecond flash x-ray sources. The resulting x-ray shadowgraphs permit the projectile velocity to be measured to within 0.2 percent. When the projectile hits the sample, the streak camera is activated, recording the shock wave velocity through the sample.

Table 2. Compositions (percent by weight) of components in pyrolite (39) and a chemically equivalent combination of key rocks and minerals (38).

Pyrolite		Model mantle		Density at 120 GPa (g/cm ³)
Formula	Per-cent	Formula	Per-cent	
(Mg _{0.916} ,Fe _{0.080} ,Ni _{0.004}) ₂ SiO ₄	52.8	(Mg _{0.915} ,Fe _{0.081} ,Ni _{0.003} ,Mn _{0.001}) ₂ SiO ₄ *	52.9	5.26
(Mg _{0.857} ,Fe _{0.139} ,Mn _{0.004})SiO ₃	35.4	(Mg _{0.852} ,Fe _{0.145} ,Mn _{0.003})SiO ₃ †	35.3	5.40
CaSiO ₃	6.4	CaSiO ₃	6.4	5.30
Al ₂ O ₃	4.6	Al ₂ O ₃	4.6	5.16
Cr ₂ O ₃	0.3	Cr ₂ O ₃ ‡	0.6	
Fe ₂ O ₃	0.3	Fe ₂ O ₃ ‡	0.2	
TiO ₂	0.2			
Total	100.0		100.0	

*Twin Sisters dunite (45). †Stillwater bronzitite (45). ‡Contained in Twin Sisters dunite.

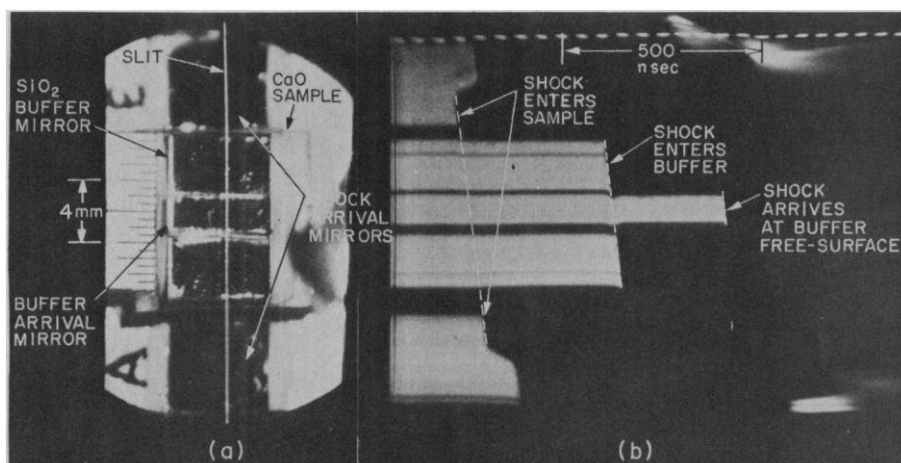


Fig. 4. Streak camera photograph of shock compression experiment on a calcia (CaO) sample. (a) Photograph of the sample assembly as seen through the streak camera, showing the position of the slit in relation to the mirrors that detect shock arrival at the driver plate-specimen interface, the sample free surface, and the SiO₂-glass buffer free surface (38). (b) Streak photograph resulting from sweeping the image of the slit horizontally (to the right), showing the extinction of light as the shock wave enters the sample and overlying buffer material. Extinction is oblique because the projectile is tilted on impact.

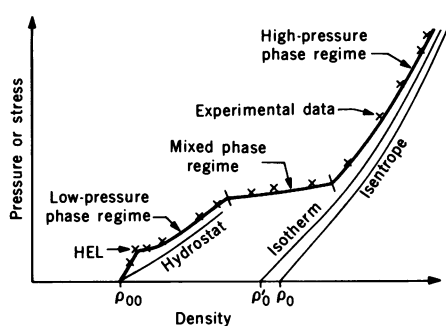


Fig. 5. Features of the Hugoniot curves of a hypothetical material, showing the relation of the Hugoniot elastic limit (HEL) to the hydrostatic compression curve (hydrostat) of a low-pressure phase of initial density ρ_{00} . As observed for most earth materials, the onset of a shock-induced phase transition occurs at the lowest pressure of the mixed phase regime, and the upper portion of the Hugoniot curve appears to correspond to the behavior of a high-pressure phase of density ρ_0 at standard conditions. The isotherm shown corresponds to the pressure-density relation of a high-pressure phase material heated to an initial density ρ_0 .

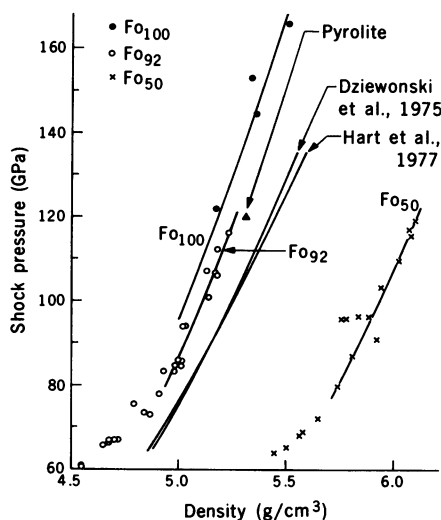


Fig. 6. Hugoniot data for Mg₂SiO₄ (Fo₁₀₀) (38), Twin Sisters dunite (Fo₉₂), and Mooihoek dunite (Fo₅₀) (45) compared to the Hugoniot density estimated for pyrolite (Table 2) and the density-pressure results for the lower mantle obtained by Dziewonski *et al.* (59) and Hart *et al.* (60) from earth free-oscillation data.

either elastic moduli and their pressure derivatives or pressure-density data, which assumes the material in the shock state can retain zero strength) constrains the possible value of deviatoric stresses associated with the shock state (14). With the notable exception of corundum and calcite (25), the shock data for most minerals, including forsterite, iron, halite, plagioclase, calcium oxide (calcia), and garnet, are in remarkable agreement with the hydrostat at pressures below those required for shock-induced transition.

A wide range of metallic elements, including Cu, Al, Mg, Ni, V, Nb, Ta, Mo, W, Re, Rh, Pd, Ir, Pt, Ag, Zn, Co, and Au, do not show evidence of phase transition under shock compression, and the 298 K isotherms or the isentropes calculated from these data are in excellent agreement with static compression and ultrasonic data (4, 8). As early as 1967, Johnson *et al.* (26) at Lawrence Livermore Laboratory demonstrated by flash x-ray experiments that solids shocked to high pressures were indeed ordered, on length scales sufficient to produce diffraction patterns corresponding to densities that agreed with those calculated from the Rankine-Hugoniot equations. In the case of simple displacive transformations, such as the transition from the α to the ϵ phase of iron or from the NaCl structure to the CsCl structure as in alkali halides and in calcia, the increase in density achieved by shock states appears to agree closely with the density increases inferred from largely static [but in one case dynamic (27)] high-pressure x-ray data.

In the case of reconstructive transformations, which occur in many of the silicates, comparison of shock data with static high-pressure phase equilibrium data demonstrates that the onset and completion of phase transformation require substantially higher than equilibrium pressures. The data for various olivines (Fig. 6), which are typical of silicates, demonstrate this discrepancy. For example, at 1000 K and equilibrium conditions, Mg₂SiO₄, the olivine magnesium end member, transforms from the olivine structure to the β -spinel structure at ~ 14 GPa; this phase in turn transforms at ~ 20 GPa to the γ -spinel phase; and at 27 GPa transition to the assemblage MgSiO₃ (perovskite) + MgO (rock salt) takes place according to static experiments (28). Along the Hugoniot curve, transformation does not begin until about 30 GPa, and complete transformation to what appear to be the high-pressure phases does not take place until shock pressures of ~ 90 GPa are

achieved. Thus over a wide pressure range the Hugoniot states appear to represent states that do not correspond to phase equilibrium. Interestingly, small amounts of the inferred high-pressure phase or phase assemblage produced by reconstructive transformation are recovered from shock experiments and meteorite impact events in the case of quartz (14), plagioclase (29), garnet (30), pyroxene (31), olivine (31), and andalusite (32). When experimentally shocked samples of such minerals as pyroxene and olivine are examined, however, there is a decided lack of evidence for reconstructive transformation under shock (33). These results and the very low yields of reconstructively produced high-pressure phases (14, 30) present an enigma.

The densities at 298 K calculated from shock wave data for Cu, Mo, Pd, Ag, and Au at a series of pressures have been compared with the densities observed in a diamond anvil high-pressure x-ray apparatus. The shock wave-derived densities thus provide an absolute pressure calibration from 6 to ~100 GPa with an uncertainty of ± 6 percent for a new generation of static high-pressure (diamond anvil) apparatuses (34).

Mantle Minerals

Since the first shock wave measurements on mantle minerals in 1958, there has been substantial advance in our detailed knowledge of the variation of elastic and anelastic properties of the earth's mantle. This has come about through the use of seismic arrays and the development of methods for calculating seismic wave forms and comparing them with observations. A large data base has been gathered from the Worldwide Standard Seismic Network and, more recently, from recordings of the earth's free oscillations by the International Digital Accelerogram Network (35). Both types of data provide a direct—but unfortunately rather low resolution—link to the density distribution in the earth.

Earlier density models of the earth required assumptions about the chemical homogeneity and adiabaticity of various regions of the earth's interior. In parallel with the better and more detailed seismological models of the earth, improvements in the design of internally heated and calibrated high-pressure apparatuses have now made it possible to produce quasi-hydrostatic environments of 15 GPa and 1200°C (36). Advances have been made in diamond anvil technology, through which compression curves of minerals can be determined to ~100

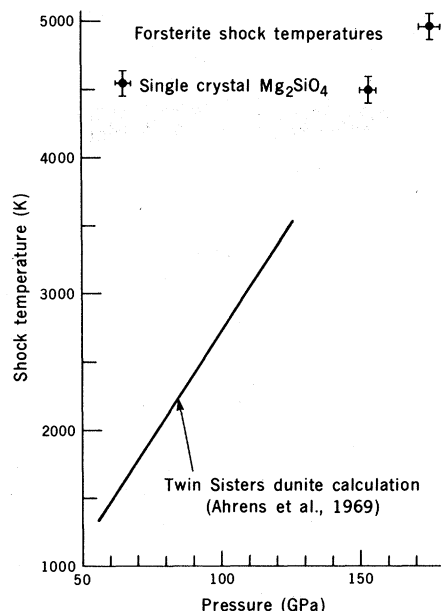


Fig. 7. Shock temperatures measured in shocked single-crystal Mg_2SiO_4 with a six-wavelength high-speed pyrometer provide experimental verification of shock temperature calculations (61). The shock temperature corresponding to the pyrolite density of 5.31 g/cm^3 at 120 GPa is ~3300 K, which is compatible with thermal models of the mantle (40).

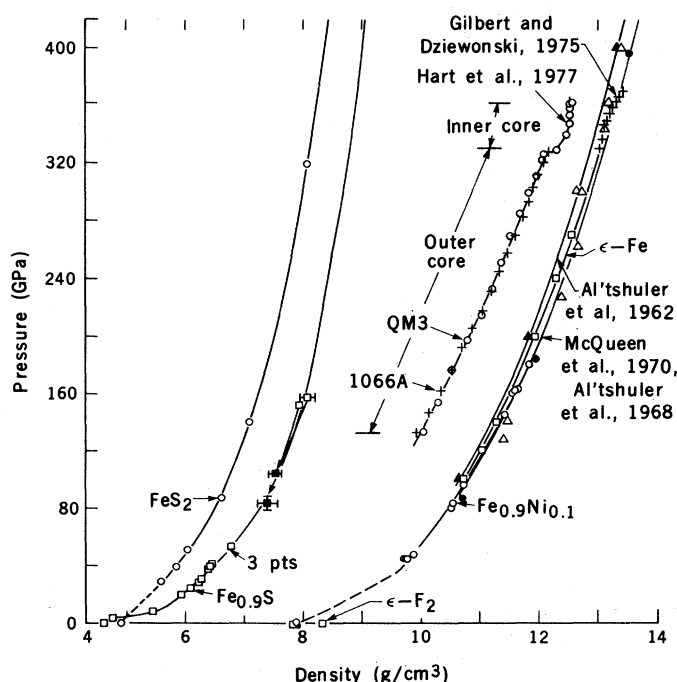
GPa and, by use of laser heating, reconnaissance phase diagram measurements can be carried out to ~26 GPa and 2000°C (37). These techniques have proved useful in comparing shock wave data with both earth measurements and other laboratory results.

The shock wave data for Twin Sisters dunite, which is 92 percent forsterite [Fo_{92} , or $(\text{Mg}_{0.92}, \text{Fe}_{0.08})_2\text{SiO}_4$], and Mooi-

hoek dunite (Fo_{45}) (Fig. 6) have been useful in inferring the approximate composition of the lower mantle, as their pressure-density relations straddle those obtained from seismology. By comparing the adiabatic pressure-density relation for the lower mantle with the dunite shock data, a lower mantle composition similar to $(\text{Mg}_{0.85}, \text{Fe}_{0.15})_2\text{SiO}_4$ (38) has been inferred. If a lower mantle composition similar to Ringwood's pyrolite model (39) (Table 2) is assumed, the shock wave data yield a density of 5.31 g/cm^3 at 120 GPa, which is considerably lower than the value of 5.42 g/cm^3 for the mantle. The temperatures assumed in this calculation are controlled mostly by the Hugoniot curve of Twin Sisters dunite, which gives ~3300 K at 120 GPa (Fig. 7). This temperature is fortuitously compatible with estimates of the lower mantle temperature (40). Thus both a pure olivine stoichiometry and a pyrolite mantle (Table 2) appear to require a slight iron or silica enrichment relative to the upper mantle (41).

An inhomogeneous mantle could result from postaccretionary mantlewide differentiation or from an inhomogeneous accretion history (42) in which the earth and other planets accreted from dust grains while the grains were condensing from the early solar nebula. In the latter model, the iron core and the refractory component of the mantle (Ca, Al, and Ti oxides and silicates) largely accreted before the other mantle minerals condensed. Thus, if the entire mantle of the earth was never homogenized by mantlewide convection,

Fig. 8. Pressure-density Hugoniot data for FeS_2 (pyrite) (55), $\text{Fe}_{0.9}\text{S}$ (pyrrhotite) (52), Fe (53), and $\text{Fe}_{0.9}\text{Ni}_{0.1}$ (54) and seismologically derived relations for the outer and inner cores of the earth. When Hugoniot data are corrected to temperatures of 3500 to 5000 K, the seismic data are compatible with a sulfur content of 9 to 12 percent by weight in a liquid outer core consisting of Fe or $\text{Fe}_{0.9}\text{Ni}_{0.1}$.



the lower mantle may be enriched in refractory minerals. The high-pressure phases of the refractory minerals such as spinel (MgAl_2O_4 ; density, 4.34 g/cm^3) and gehlenite ($\text{Ca}_2\text{Al}_2\text{SiO}_7$; density, 4.43 g/cm^3) (43) have significantly higher zero-pressure densities than the high-pressure phases corresponding to an olivine and pyroxene composition, MgSiO_3 (perovskite) + MgO (rock salt). Shock wave data for calcia (44) and hedenbergite, $(\text{Ca,Fe})_2\text{Si}_2\text{O}_6$ (45), give densities that are consistent with a refractory-rich lower mantle.

The Core

Much of what has been inferred about the composition of the earth's core has been based on comparisons of seismologically derived velocity data with laboratory compression results obtained in shock wave experiments. In 1952 Birch (46) and later Knopoff and McDonald (47) observed, on the basis of shock wave data, that the incorporation of a cosmochemically abundant element such as silicon or carbon with iron might account for the density of the earth's outer core being lower, by about 8 to 10 percent, than that of pure iron (Fig. 8). Based on the model of a CC1 carbonaceous chondrite composition for the earth and the realization that an average rise of $\sim 2000 \text{ K}$ in the earth's temperature would result from core formation from a homogeneously accreted earth, the hypothesis that silicon was a major element in the outer core (~ 11 percent by weight) received wide acceptance (39). Shock wave experiments on Fe-Si alloys showed (48) that a silicon content of 14 to 20 percent by weight would be required to reduce the density (at 130 GPa) from approximately 11 g/cm^3 (for pure iron) to the 10 g/cm^3 observed for the outermost core. A major difficulty with this hypothesis is that such an Fe-Si alloy would be in chemical disequilibrium with the overlying iron silicate-bearing mantle.

Two hypotheses that have recently been examined by shock wave studies of appropriate minerals are that the core contains appreciable quantities of oxygen (49) and that it contains large amounts of sulfur (50). An oxygen- or sulfur-bearing core would not necessarily be in disequilibrium with a silicate mantle. These shock wave data make the hypothesis of silicon in the core appear less likely (39). Recent shock wave data for FeO (51) show that ~ 8 percent oxygen could be present in the core, whereas shock wave data for FeS and FeS_2 (52)

permit 9 to 12 percent sulfur. Ringwood (49) pointed out that accretion of substantial quantities of either oxygen or sulfur in the earth's core would require that the hydrogen abundance during accretion of the earth was a factor of 10^2 less than that in the present solar chromosphere.

The relative density of the solid inner core, although poorly constrained by seismological data, may be some 10 percent greater than that of the liquid outer core. At present, it appears that the inner core, which has only 5 percent of the mass of the core, may be composed of nearly pure iron.

Conclusions

Shock wave experiments provide absolute pressure-density and, more recently, temperature data for minerals at pressures that encompass the entire range present in the earth—up to 370 GPa or 3.7 Mbar. Shock data for metals, silicates, oxides, and sulfides agree well with available static high-pressure x-ray data for the density of both low-pressure and shock-induced high-pressure phases. Dynamic experiments demonstrate that major phase changes can take place on a submicrosecond time scale in many materials of geophysical interest. The onsets of phase transitions correspond well to those inferred from static high-pressure x-ray data when they are of the displacive type (for example, the α to the ϵ phase of iron), whereas for reconstructive-type transformations, which often occur in silicates, higher than equilibrium pressures are required under shock to initiate transformation.

The density of a hypothetical mixture of dunite, bronzite, wollastonite, and corundum, which closely approximates Ringwood's estimate of the bulk composition of the mantle pyrolite at a pressure of 120 GPa, was calculated from shock wave data. The theoretical density of 5.31 g/cm^3 obtained for a pressure of 120 GPa is significantly below the value of 5.42 g/cm^3 inferred at this pressure in the mantle (depth, 2600 km) from seismological data. The increase in density over that inferred for an olivine-rich pyrolite could be due to enrichment of the more refractory compounds such as CaO , $\text{Ca}_2\text{Al}_2\text{SiO}_7$, and MgAl_2O_4 , which high-pressure x-ray and shock wave data show can have densities equivalent to or higher than those based on an olivine stoichiometry on transformation to high-pressure phases.

Because the density of the earth's outer core is some 10 percent less than that

of pure iron, it is possible to obtain constraints on the amounts of geochemically plausible light elements that may be dissolved in a liquid iron core. Shock wave experiments have shown that the outer core density is compatible with some 9 to 12 percent sulfur or some 10 percent oxygen. The presence of either of these elements in the core allows the core to be in chemical equilibrium with the overlying mantle and the earth as a whole to be close to the composition of the heavy nonvolatile elements in the sun.

References and Notes

1. The international unit of pressure commonly used in shock wave research is the gigapascal (GPa), which is equivalent to 10 kilobars, 0.1 megabar, 10^{10} dynes per square centimeter, or 9869 atmospheres.
2. D. S. Hughes and R. M. McQueen, *Trans. Am. Geophys. Union* **39**, 959 (1958).
3. W. P. Bridgman, *Proc. Am. Acad. Arts Sci.* **76**, 55 (1948).
4. J. M. Walsh and R. H. Christian, *Phys. Rev.* **97**, 1544 (1955).
5. S. Minshall, *ibid.* **98**, 271 (1955).
6. J. C. Jamieson and A. N. Lawson, *J. Appl. Phys.* **33**, 776 (1962).
7. J. C. Jamieson, *Science* **139**, 762 (1963). A complete x-ray pattern of this structure was reported by T. Takahashi and W. A. Bassett [*ibid.* **145**, 483 (1964)].
8. L. V. Al'tshuler, K. K. Krupnikov, M. I. Brazhnik, *Sov. Phys. JETP* **34**, 614 (1958); L. V. Al'tshuler, K. K. Krupnikov, B. A. Ledenev, V. I. Zhuchikhin, M. I. Brazhnik, *Zh. Eksp. Teor. Fiz.* **34**, 4 (1958).
9. P. S. DeCarli and J. C. Jamieson, *Science* **133**, 1821 (1961); L. F. Trueb, *J. Appl. Phys.* **39**, 4207 (1968).
10. M. N. Pavlovskii and V. P. Drakin, *JETP Lett.* **4**, 116 (1966).
11. V. N. German, N. N. Orlova, M. N. Pavlovskii, L. A. Tarasova, R. F. Trunin, *Izv. Earth Phys.* **8**, 487 (1975); L. V. Al'tshuler, M. A. Poderets, G. V. Sinalson, R. F. Trunin, *Solid State Phys.* **15**, 5 (1973).
12. R. G. McQueen and S. P. Marsh, *Geol. Soc. Am. Mem.* **97** (1966), p. 154.
13. R. G. McQueen, J. C. Jamieson, S. P. Marsh, *Science* **155**, 1401 (1967); R. K. Linde and P. S. DeCarli, *J. Chem. Phys.* **50**, 1 (1969).
14. P. S. DeCarli and D. J. Milton, *Science* **147**, 144 (1965); J. D. Kleeman and T. J. Ahrens, *J. Geophys. Res.* **78**, 5954 (1973); E. C. T. Chao, J. T. Fahey, T. Littler, *ibid.* **67**, 419 (1962).
15. L.-G. Liu, *Phys. Earth Planet. Inter.* **9**, 338 (1974); *ibid.* **10**, 167 (1975); *Science* **199**, 422 (1978).
16. *Engineering with Nuclear Explosives* (CONF 700101, U.S. Atomic Energy Commission, Oak Ridge, Tenn., 1970), vols. 1 and 2; E. Teller, W. K. Talley, G. H. Higgins, G. W. Johnson, *The Constructive Uses of Nuclear Explosions* (McGraw-Hill, New York, 1968).
17. H. C. Rodean, *Nuclear Explosion Seismology* (TID 25572, U.S. Atomic Energy Commission, Oak Ridge, Tenn., 1972).
18. "Protecting MX against the new Soviet missiles," *Energy and Technology Review*, 18 October 1978; report UCRL 5200-78-10, Lawrence Livermore Laboratory, University of California, Berkeley, 1978.
19. G. E. Duvall and G. R. Fowles, in *High Pressure Physics and Chemistry*, R. S. Bradley, Ed. (Academic Press, New York, 1963), vol. 2, pp. 209-291.
20. L. V. Al'tshuler, B. N. Moiseyev, L. V. Popov, G. V. Simakov, R. F. Trunin, *Zh. Eksp. Teor. Fiz.* **54**, 785 (1968).
21. A. H. Jones, W. M. Isbell, C. J. Maiden, *J. Appl. Phys.* **37**, 3492 (1966).
22. T. Neal, *ibid.* **46**, 2521 (1975).
23. G. A. Lyzenga and T. J. Ahrens, *Bull. Am. Phys. Soc.* **24**, 714 (1979); *Rev. Sci. Instrum.*, in press; S. B. Kormer, *Sov. Phys. Usp.* **11**, 229 (1968).
24. R. A. Graham and O. E. Jones, Rep. SC-R-68-1857, Sandia Laboratories, Albuquerque, N.M. (1968).
25. T. J. Ahrens and R. K. Linde, in *Behavior of Dense Media Under High Dynamic Pressure*, J. Berger, Ed. (Gordon & Breach, New York, 1968), p. 325.

26. Q. Johnson, R. N. Keeler, J. W. Lyle, *Nature (London)* **213**, 1114 (1967).
27. Q. Johnson and A. C. Mitchell [*Phys. Rev. Lett.* **29**, 1369 (1972)] demonstrated that during shock compression at 24.5 GPa, BN (initially in the low-pressure phase) exhibits the x-ray diffraction pattern of the high-pressure, wurtzite phase.
28. L.-G. Liu, *Nature (London)* **262**, 770 (1976).
29. O. B. James, *Science* **165**, 1005 (1969).
30. E. K. Graham and T. J. Ahrens, *J. Geophys. Res.* **78**, 375 (1973); L.-G. Liu, *Earth Planet. Sci. Lett.* **26**, 425 (1975).
31. J. V. Smith and B. Mason, *Science* **168**, 832 (1970); M. Madon and J.-P. Poirer, *ibid.* **207**, 66 (1980).
32. H. Schneider and V. Hornemann, *Phys. Chem. Miner.* **1**, 257 (1977).
33. R. Jeanloz, unpublished manuscript; S. S. Pollock and P. S. DeCarli, *Science* **165**, 591 (1969); R. Jeanloz and T. J. Ahrens, *Geol. Soc. Am. Abstr. Programs* **9**, 1306 (1977).
34. H. K. Mao, P. M. Bell, J. W. Shaner, D. J. Steinberg, *J. Appl. Phys.* **49**, 3276 (1978).
35. D. Agnew, J. Berger, R. Buland, W. Farrell, F. Gilbert, *Eos* **57**, 180 (1976).
36. S. Akimoto, M. Akaogi, K. Kawada, O. Nishigawa, *Am. Geophys. Union Monogr.* **19** (1976), p. 399.
37. P. M. Bell and H. K. Mao, in *High Pressure Research: Applications in Geophysics*, M. Manghani and S. Akimoto, Eds. (Academic Press, New York, 1977), p. 509; L. Ming and W. A. Bassett, *Rev. Sci. Instrum.* **45**, 1115 (1974).
38. I. Jackson and T. J. Ahrens, *J. Geophys. Res.* **84**, 3039 (1979).
39. A. E. Ringwood, *Composition and Petrology of the Earth's Mantle* (McGraw-Hill, New York, 1975), p. 188. The term pyrolyte (pyroxene + olivine \pm pyrope garnet rock) was coined to represent the upper mantle composition that yields, with differing amounts of partial melting and under a range of temperature and pressure conditions, a wide range of the igneous rocks that originate from the upper mantle.
40. T. D. Stacey, *Physics of the Earth* (Wiley, New York, ed. 2, 1977).
41. D. L. Anderson, C. Sammis, T. Jordan, *Science* **171**, 1103 (1971).
42. K. K. Turekian and S. P. Clark, Jr., *Earth Planet. Sci. Lett.* **6**, 346 (1969).
43. L.-G. Liu, *ibid.* **40**, 401 (1978); *ibid.* **41**, 398 (1978).
44. R. Jeanloz, T. J. Ahrens, H. K. Mao, P. M. Bell, *Bull. Am. Phys. Soc.* **24**, 724 (1979); *Science* **206**, 829 (1979).
45. R. G. McQueen, S. P. Marsh, J. N. Fritz, *J. Geophys. Res.* **72**, 4999 (1967); G. V. Simakov *et al.* (55).
46. F. Birch, *J. Geophys. Res.* **57**, 227 (1952).
47. L. Knopff and G. T. F. MacDonald, *Geophys. J. R. Astron. Soc.* **3**, 68 (1960).
48. S. B. Kormer and A. I. Funtikov, *Bull. Acad. Sci. USSR Earth Phys. No. 5* (1956); A. S. Balchan and G. R. Cowan, *J. Geophys. Res.* **71**, 3577 (1966).
49. A. E. Ringwood, *Geochem. J.* **11**, 111 (1978).
50. V. R. Murthy and H. T. Hall, *Phys. Earth Planet. Inter.* **2**, 276 (1970).
51. R. Jeanloz, T. J. Ahrens, M. Somerville, *Eos* **60**, 387 (1979); R. Jeanloz and T. J. Ahrens, in preparation.
52. T. J. Ahrens, *J. Geophys. Res.* **84**, 985 (1979).
53. D. J. Andrews, *J. Phys. Chem. Solids* **34**, 825 (1973); H. K. Mao, W. A. Bassett, T. Takahashi, *J. Appl. Phys.* **38**, 272 (1967).
54. R. G. McQueen and S. P. Marsh, *J. Geophys. Res.* **71**, 1751 (1966); L. V. Al'tshuler, G. V. Simakov, R. F. Trunin, *Izv. Earth Phys.* **1**, 3 (1968).
55. G. V. Simakov, M. N. Palovskii, N. G. Kalashnikov, R. F. Trunin, *Izv. Acad. Sci. USSR Phys. Solid Earth* **8**, 11 (1974).
56. G. F. Davies and E. S. Gaffney, *Geophys. J. R. Astron. Soc.* **33**, 165 (1973).
57. R. G. McQueen, J. N. Fritz, S. P. Marsh, *J. Geophys. Res.* **68**, 2319 (1963); J. Wackerle, *J. Appl. Phys.* **33**, 922 (1962); L. V. Al'tshuler, R. F. Trunin, G. V. Sinalson, *Izv. Akad. Nauk SSSR Fiz. Zemli. No. 10* (1968).
58. C. E. Ragen III, M. G. Silbert, B. C. Diven, *J. Appl. Phys.* **48**, 2860 (1977).
59. A. M. Dziewonski, A. L. Hales, E. R. Lapwood, *Phys. Earth Planet. Inter.* **10**, 12 (1975).
60. R. S. Hart, D. L. Anderson, H. Kanamori, *J. Geophys. Res.* **82**, 1647 (1977).
61. T. J. Ahrens, A. E. Ringwood, D. L. Anderson, *Rev. Geophys. Space Phys.* **7**, 667 (1968). Shock temperature measurements are from G. A. Lyzenga and T. J. Ahrens (unpublished data). Experiments were performed with the Lawrence Livermore Laboratory light-gas gun apparatus.
62. I am grateful for the critical comments of R. Jeanloz, D. L. Anderson, and two anonymous reviewers of this article. Supported under NSF grants EAR 75-15006A01, EAR 77-23156, and EAR 78-12942. This is Contribution 3259, Division of Geological and Planetary Sciences, California Institute of Technology.

Volcanic Activity and Climatic Changes

Reid A. Bryson and Brian M. Goodman

Since before the time of Aristotle, it has been known that climatic variation is in part a function of solar radiation intensity as it varies with latitude. In the last two centuries the idea has also emerged that climatic variation in time

the past century have been based on the assumption that the transparency of the cloudless atmosphere has varied—specifically, as related to this article, in response to variations of volcanically produced turbidity (2).

Summary. Radiocarbon dates of volcanic activity suggest variations that appear to be related to climatic changes. Historical eruption records also show variations on the scale of years to centuries. These records can be combined with simple climatic models to estimate the impact of various volcanic activity levels. From this analysis it appears that climatic prediction in the range of 2 years to many decades requires broad-scale volcanic activity prediction. Statistical analysis of the volcanic record suggests that some predictability is possible.

might be related to variations in ground-level solar intensity (I). These variations could be due to either changes in the solar output or changes in the transparency of the atmosphere. Indeed, the more successful simulations of the course of hemispheric or zonal temperatures over

In part, these models help distinguish between variations of direct-beam solar radiation observed at the surface and variations produced by volcanic debris changing the atmospheric transparency. For example, the sensitivity of the hemispheric mean surface temperature to a 1

percent change in the solar constant is about 1.2 to 2.0 K (2). Since the measured values of direct solar radiation decreased about 5 percent during the period 1945 to 1975 (3), the surface mean temperature should have decreased 6 to 10 K during this time if only the solar constant varied (4). This is clearly much larger than the 0.3 K or so that was observed (5). On the other hand, if the turbidity of the atmosphere varied enough to reduce the direct beam at the surface by 5 percent, the surface mean temperature should have decreased by about 0.85 K, all other factors being ignored. This is because increased turbidity increases the diffuse radiation almost as much as it decreases the direct beam. Correcting this value for the effect of increasing carbon dioxide (about 12 parts per million), which gives a temperature increase of about 0.30 to 0.35 K (6), results in a calculated decrease in hemispheric mean surface temperature of 0.50 to 0.55 K. This is much closer to the observed decrease than the value obtained with the assumption of decreased solar constant. If we also take into account the lag produced by heat storage in the oceans, the match is very close.

The reasoning above with the aid of a physical model indicates that it will be necessary to estimate future levels of

Reid Bryson is the director and Brian Goodman is a research assistant at the Institute for Environmental Studies, University of Wisconsin, Madison 53706. This article is based on a paper presented at the AAAS annual meeting in Houston, Texas, in January 1979.